HHS Public Access

Author manuscript

Oncogene. Author manuscript; available in PMC 2022 July 24.

Published in final edited form as:

Oncogene. 2022 February ; 41(8): 1190–1202. doi:10.1038/s41388-021-02157-x.

SOX2 Mediates Metabolic Reprogramming of Prostate Cancer Cells

Larischa de Wet[1], **Anthony Williams**[2], **Marc Gillard**[2], **Steven Kregel**[1], **Sophia Lamperis**[3], **Lisa C. Gutgesell**[3], **Jordan E. Vellky**[3], **Ryan Brown**[3], **Kelly Conger**[4], **Gladell P. Paner**[5], **Heng Wang**[6], **Elizabeth E. Platz**[7], **Angelo M. De Marzo**[8], **Ping Mu**[9], **Jonathan L. Coloff**[4], **Russell Z. Szmulewitz**[2], **Donald J. Vander Griend**[3,*]

[1]Committee on Cancer Biology; The University of Chicago; Chicago, IL 60637; USA

[2]Department of Medicine, Section of Hematology/Oncology; The University of Chicago; Chicago, IL 60637; USA

[3]Department of Pathology; The University of Illinois at Chicago; Chicago, IL 60637; USA

[4]Department of Physiology and Biophysics; The University of Illinois at Chicago; Chicago, IL 60637; USA

[5]Department of Pathology; The University of Chicago; Chicago, IL 60637; USA

[6]Division of Epidemiology and Biostatistics, School of Public Health; The University of Illinois at Chicago; Chicago, IL 60607; USA

[7]Department of Epidemiology, Johns Hopkins Bloomberg School of Public Health, Baltimore, MD 21205

[8]Departments of Pathology, Urology, and Oncology, and the Brady Urological Research Institute and the Sidney Kimmel Comprehensive Cancer Center at Johns Hopkins; Johns Hopkins University; Baltimore, MD 21218; USA

[9]Department of Molecular Biology; University of Texas Southwestern Medical Center; Dallas, TX 75390; USA

Abstract

[*]*Please address all correspondence to*: Donald J. Vander Griend, Ph.D., The University of Illinois at Chicago Department of Pathology, 840 S. Wood Street, 130 CSN, MC847, Chicago, IL 60612; dvanderg@uic.edu.

AUTHOR CONTRIBUTIONS

Conceptualization: D.J.V.G., L.D.W., S.K., J.C., R.Z.S.
Methodology: D.J.V.G., L.D.W., M.G., S.K., S.L.
Formal Analysis: D.J.V.G., L.D.W., A.W., M.G., S.K., G.P., H.W.
Investigations: D.J.V.G., L.D.W., A.W., M.G., S.K., S.L., L.G., J.V., R.B., K.C.
Resource: E.P, A.M.D., P.M.
Data Curation: D.J.V.G., L.D.W., A.W., G.P.
Writing and Editing: D.J.V.G., L.D.W.
Supervision: D.J.V.G.

Conflicts of Interest: None

DECLARATION OF INTERESTS

The authors declare no competing interests.

New strategies are needed to predict and overcome metastatic progression and therapy resistance in prostate cancer. One potential clinical target is the stem cell transcription factor SOX2, which has a critical role in prostate development and cancer. We thus investigated the impact of SOX2 expression on patient outcomes and its function within prostate cancer cells. Analyses of SOX2 expression among a case-control cohort of 1028 annotated tumor specimens demonstrated that SOX2 expression confers a more rapid time to metastasis and decreased patient survival after biochemical recurrence. SOX2 ChIP-Seq analyses revealed SOX2 binding sites within prostate cancer cells which differ significantly from canonical embryonic SOX2 gene targets, and prostate-specific SOX2 gene targets are associated with multiple oncogenic pathways. Interestingly, phenotypic and gene expression analyses after CRISPR-mediated deletion of *SOX2* in castration-resistant prostate cancer cells, as well as ectopic *SOX2* expression in androgen-sensitive prostate cancer cells, demonstrated that SOX2 promotes changes in multiple metabolic pathways and metabolites. SOX2 expression in prostate cancer cell lines confers increased glycolysis and glycolytic capacity, as well as increased basal and maximal oxidative respiration and increased spare respiratory capacity. Further, SOX2 expression was associated with increased quantities of mitochondria, and metabolomic analyses revealed SOX2-associated changes in the metabolism of purines, pyrimidines, amino acids and sugars, and the pentose phosphate pathway. Analyses of SOX2 gene targets with central functions metabolism *(CERK*, *ECHS1*, *HS6SDT1*, *LPCAT4*, *PFKP*, *SLC16A3*, *SLC46A1*, and *TST)* document significant expression correlation with SOX2 among RNA-Seq datasets derived from patient tumors and metastases. These data support a key role for SOX2 in metabolic reprogramming of prostate cancer cells and reveal new mechanisms to understand how SOX2 enables metastatic progression, lineage plasticity, and therapy resistance. Further, our data suggest clinical opportunities to exploit SOX2 as a biomarker for staging and imaging, as well as a potential pharmacologic target.

Keywords

prostate cancer; SOX2; androgen receptor; stem cell; metabolism; metastasis

INTRODUCTION

Metastatic prostate cancer is a significant health problem, and novel strategies are needed to understand and overcome cellular mechanisms of therapeutic resistance. Recent studies suggest an important role for the stem cell regulator and Yamanaka factor, sex determining region Y-box 2 (SOX2) in mediating resistance to hormone therapy [1–3]. SOX2 is a member of the SOXB1 subfamily of SOX transcription factors and is an essential transcriptional regulator in stem cell pluripotency [4], and the interactions of various co-factors with SOX2 enables transcriptional versatility during developmental processes and into adulthood where SOX2 functions to maintain adult stem cell populations [5]. However, the mechanisms through which SOX2 regulates prostate cancer progression and therapy resistance remain unclear, hampering the development of novel clinical strategies to predict, prevent, and reduce the metastatic progression of prostate tumors.

Interest in the function of SOX2 in cancer has uncovered key roles in proliferation, evasion of cell death, and activation of cell invasion and metastasis within several cancer types

including breast, lung, and gastric cancers [6–14]. Further, SOX2 increases expression of putative cancer stem cell markers in ovarian, lung, and pancreatic cancers [15–17]. These putative cancer stem cells may acquire tumor-initiating and self-renewal properties by reactivating stem cell markers or pluripotency factors [18].

More recently, numerous groups identified a role for SOX2 in promoting therapy resistance and lineage plasticity of prostate cancer cells, particularly in the context of androgen receptor (AR) signaling blockade. We reported increased SOX2 expression within a series of prostate cancer cell lines and among tumor xenografts upon acquisition of resistance to AR signaling blockade using the anti-androgen enzalutamide or host castration, and determined that ectopic SOX2 expression is sufficient for castration-resistant tumor formation [2]. Depletion of endogenous SOX2 in castration-resistant cell lines inhibits growth, and the typical co-factors NANOG and OCT4 are not expressed in SOX2-positive cancer cells [2]. In accordance with our findings, Mu et al. reported increased SOX2 expression and concomitant resistance to enzalutamide within prostate cancer cells after depletion of p53 and RB; inhibition of SOX2 expression within these lines re-established sensitivity to AR pathway blockade [3]. Finally, we and others documented SOX2 expression within a subset of primary prostate tumors, with a correlative increase in the percentage of SOX2-positive tumors with increasing Gleason grade [2, 19–22]. Interestingly, tumor SOX2 expression is binary—tumors are either uniformly SOX2-positive or SOX2-negative, with a lack of admixed SOX2-positive cells characteristic of cancer stem-like cells [2]. Collectively, these data implicate a central and critical role for SOX2 in promoting resistance to AR-targeted therapies, suggest that tumor SOX2 expression may confer poor patient prognosis, and indicate that SOX2 may interact with novel co-factors in prostate cancer cells to regulate alternate pathways beyond pluripotency and differentiation. Thus, mechanistic understanding of SOX2 gene targets and pathway regulation within prostate cancer cells has the potential to identify and/or prioritize therapeutic approaches to prevent and overcome prostate cancer therapy resistance.

In this study, we report the impact of tumor SOX2 expression on prostate cancer metastasis and patient survival and demonstrate that SOX2 mediates both glycolytic and oxidative phosphorylation metabolic pathways in cell-based models. Further, we identify numerous SOX2-mediated pathways in prostate cancer cells that are not associated with canonical SOX2 function in embryonic stem cells, suggesting the relocating of SOX2 to novel oncogenic drivers during prostate tumor progression. These data collectively implicate novel SOX2 transcriptional activity and gene targets as critical mediators and potential pharmacologic targets driving prostate cancer progression and therapy resistance.

RESULTS

SOX2 Expression in Primary Prostate Tumors is Associated with Rapid Time to Metastasis and Prostate Cancer-Specific Mortality

Previously reported data from our group demonstrate SOX2 expression in a portion of basal cell populations within benign epithelia. Pre-malignant, high-grade prostatic intra-epithelial neoplasia (PIN) lesions show mixed basal and luminal epithelial cell SOX2 expression [2]. Analyses of primary prostate tumors document SOX2 expression within a subset

of tumors, with a correlative increase in the percentage of SOX2-positive tumors with increasing Gleason grade [2]. Interestingly, tumor SOX2 expression is binary, and we did not observe tumors with heterogeneous SOX2 expression (i.e., containing mixed SOX2-positive and SOX2-negative tumor cells) [2]. This observation led us to hypothesize that tumor SOX2 expression confers an increased risk of cancer progression and worse overall patient prognosis at the time of surgery. To test this hypothesis, SOX2 immunohistochemistry (IHC) was performed in a set of annotated tissue microarrays (TMAs) from the Brady Recurrence Nested Case-Control Study provided by the Prostate Cancer Biorepository Network, composed of 1,028 tumor tissues from 742 prostate cancer patients who underwent radical retropubic prostatectomy for clinically localized prostate cancer at Johns Hopkins University Medical Center during 1993–2001 [23, 24]. In this cohort, “Cases” refer to patients that biochemically recurred, whereas “Controls” are patients who did not recur by the date of the matched case’s recurrence. As expected, SOX2 expression was found in both benign and malignant tissues (Figure 1A, Supplemental Figure 1), consistent with previous findings reported by our group [2, 25]. After SOX2 IHC staining, pathologic analyses, and elimination of samples with incomplete annotation or stained material, 477 cases of biochemical recurrence (BCR) and 248 control cases remained for statistical analyses (Supplemental Table 1). As expected, there were no significant associations between BCR and control groups based upon age, prostate-specific antigen (PSA) at surgery, race, or pathological extension (Supplemental Table 1). However, significant differences between BCR and control groups were observed for Gleason score post-radical prostatectomy (RP), years to BCR, surgical margin status, local recurrence, salvage treatment, metastasis, overall death, and prostate cancer-specific death.

Analyses of SOX2 expression revealed multiple notable observations. First, SOX2 tumor expression among Case-Control tumors was not significantly associated with tumor Gleason Grade ($p=0.81$); this observation demonstrates that SOX2 expression does not independently promote increased tumor grade. Second, there were no significant correlations between tumor SOX2 expression and BCR, years to BCR, surgical margin, pathologic extension, local recurrence, or salvage treatment (Table 1). Third and most interestingly, further analyses demonstrated that patients with SOX2-positive tumors had a more rapid time to radiographic metastasis formation after BCR as well as a higher prevalence of prostate cancer-specific death and overall death than patients with SOX2-negative tumors (Table 1, Figure 1B). A Cox proportional hazards model combining age, PSA, Gleason grade, extraprostatic extension, and seminal vesicle invasion demonstrated a significant association of tumor SOX2 expression with metastasis risk ($HR=1.496$, $p=0.0369$), in addition to expected metastatic risk factors of Gleason grade, extraprostatic extension, and seminal vesicle invasion (Figure 1C). These data demonstrate an increased propensity of SOX2-positive tumors for metastasis and prostate cancer-specific death and suggest that SOX2 expression may be associated with therapy resistance after metastatic colonization and biochemical recurrence.

SOX2 ChIP-Seq in Castration-Resistant Prostate Cancer (CRPC) Cells Reveals Multiple Non-Stem Cell Gene Targets

A correlation between SOX2 expression and a more rapid time to metastasis with decreased survival supports a hypothesis whereby SOX2 expression promotes resistance to anti-androgen therapies and progression to castration-resistant disease [2, 3]. To begin mechanistically defining the function of SOX2 in prostate cancer cells and how it contributes to therapeutic resistance, we performed paired SOX2 chromatin immunoprecipitation-sequencing (ChIP-Seq) and RNA-sequencing (RNA-Seq) on a SOX2-positive CRPC cell line, CWR-R1, to determine which genes SOX2 binds and potentially regulates. To identify novel prostate cancer-specific SOX2 gene targets in CWR-R1 cells distinct from known SOX2 stem cell genes, we conducted parallel SOX2 ChIP-Seq and RNA-Seq in the WA01 embryonic stem cell line and compared results to identified SOX2 targets from CWR-R1 cells [26, 27]. Motif analyses of SOX2-bound genes demonstrated strong homology between the SOX2 binding motif in CWR-R1 and the canonical SOX2 binding sequence (Figure 2A). Analysis of SOX2 ChIP-Seq revealed that >53% of SOX2 peaks were within protein coding genes (n=3,561; Figure 2B) and that SOX2 bound predominantly within 5,000 bp upstream of the transcription start site of these protein coding genes (Figure 2B, SOX2-bound genes are in Supplemental Table 2) [28]. RNA expression of SOX2-bound genes was predominantly high, with 87.7% of genes having an mRNA expression of transcripts per million (TPM) > 10, indicating that SOX2 binding is associated with active transcription rather than gene repression.

Comparison of SOX2 binding between CWR-R1 cancer cells and WA01 human embryonic stem cells demonstrated that, of the 3,561 genes bound by SOX2 in CWR-R1 cells, 77.6% (N=2,763) were unique to prostate cancer cells, representing potentially novel SOX2 gene targets in prostate cancer cells (Figure 2B). Of the 1,540 genes bound by SOX2 in WA01, 51.8% (N=798) were also bound by SOX2 within CWR-R1 prostate cancer cells. However, additional analyses of overlapping SOX2 target genes between CWR-R1 and WA01 cells demonstrated that SOX2 bound at distinct, non-overlapping locations (i.e., at least 10 bp apart) within 93.4% (N=745) of the 798 overlapping gene targets (Figure 2B), suggesting differential regulation of shared SOX2-bound genes between CWR-R1 CRPC cells and WA01 embryonic stem cells. Non-stem cell gene regulation by SOX2 was further supported by lack of canonical SOX2-binding partners *OCT4* and *NANOG* expression in CRPC cells compared to embryonic stem cells (Figure 2C) [2]. Notable SOX2-bound genes with robust expression in CRPC cells included *BCL2, EZH2, FGFR3, FOXA1, KLK3/PSA, KRAS, MET, TGFRB1, IKZF1, CTNNB1, PARP1*, and *ONECUT2* (Figure 2D). It should be noted that promoter binding by SOX2 does not necessarily imply transcriptional regulation.

To elucidate potential signaling pathways regulated by SOX2, we compared SOX2-bound genes using Ingenuity Pathway Analysis (IPA). Analyses demonstrated that SOX2 target genes were associated with cancer signaling pathways in CWR-R1 cells to a greater extent than in WA01 hESCs (Figure 2E), congruent with clinical data demonstrating an association between tumor SOX2 expression and increased metastasis in patients with BCR (Figure 1). Collectively, the non-canonical and unique gene targeting of SOX2 in CWR-R1 cells suggests alternate, non-stem cell functions for SOX2 in prostate cancer cells

as well as potentially novel transcriptional binding partners for SOX2. This large number of unique SOX2-bound genes in prostate cancer cells led us to further examine the role of non-canonical stem cell functions for SOX2 in CRPC cells.

SOX2 Deletion in Castration-Resistant CWR-R1 Cells Decreases Cell Growth and Invasion

We previously demonstrated that constitutive expression of SOX2 in the hormone-sensitive LAPC4 cell line is sufficient to enable castration-resistant tumor formation, and Mu et al. demonstrated that SOX2 depletion in LNCaP-RB/p53-deficient cells abrogates enzalutamide resistance [2, 3]. To more precisely elucidate SOX2-mediated genes conferring therapy resistance, we deleted *SOX2* expression in CWR-R1 CRPC cells using CRISPR-Cas9 gene editing. Targeted *SOX2* deletion (hereafter referred to as $SOX2^{KO}$) resulted in non-detectable SOX2 protein expression, as well as significant SOX2 mRNA transcript reduction, among multiple clonal lines (Figure 3A). Importantly, *SOX2* deletion did not impact expression of AR and AR-V7, a common splice variant implicated in enzalutamide resistance [29], between different clones and AR signaling conditions (Figure 3A). As anticipated, loss of SOX2 expression led to increased sensitivity to enzalutamide treatment (Figure 3B, Supplemental Figure 2A). Interestingly, $SOX2^{KO}$ cells also demonstrated decreased growth under control conditions of vehicle treatment (Figure 3B). Cell cycle and bromodeoxyuridine (BrdU) analysis demonstrated that control and $SOX2^{KO}$ cells had a similar cell-cycle distribution when treated with vehicle, but $SOX2^{KO}$ cells had fewer cells in the S-phase when treated with enzalutamide and appeared to arrest in the G_1 phase (Figure 3C).

To further examine the impact of *SOX2* deletion in CRPC CWR-R1 cells, we also performed a transwell migration assay to determine the migratory capacity of $SOX2^{KO}$ cells. $SOX2^{KO}$ cells had significantly decreased migration capacity compared to control cells (Figure 3D), further supporting a potential role in metastasis whereby patients with tumor SOX2 expression exhibit a decreased time to metastasis. Decreased growth of $SOX2^{KO}$ cells (in the absence of enzalutamide) compared to control cells was not due to increased apoptosis, as measured by propidium iodide exclusion, TUNEL microscopy, and apoptosis/necrosis assays (Figure 3E). In vivo tumor xenografting of control and $SOX2^{KO}$ cells in hormonally-intact male nude mice demonstrated that *SOX2* deletion resulted in significantly decreased tumor growth and increased survival compared to controls (Figure 3F). These data validate previous data demonstrating SOX2-mediated dependency under AR pathway-inhibited conditions and also highlight potentially novel AR-independent roles for SOX2 in regulating cell growth [2, 3].

SOX2 is Associated with Changes in Cellular Metabolism in Prostate Cancer Cells, Tumors, and Metastases

The observation that $SOX2^{KO}$ reduces prostate cancer cell growth under conditions where AR signaling is intact prompted us to identify SOX2-mediated mechanisms leading to fewer cells over time. Remarkably, the SOX2-associated decrease in cell growth occurred without increasing cell death or changes in $G_1/S/G_2$ cell-cycle distribution (Figure 3C and E). To determine the genes regulated by SOX2, we performed RNA-Seq on CWR-R1 control cells and $SOX2^{KO}$ cells with intact AR signaling and identified 3,230 differentially expressed

genes (DEGs) (Figure 4A; control vs. $SOX2^{KO}$ RNA-Seq gene lists are in Supplemental Table 3). Candidate SOX2 effector genes were prioritized by limiting to SOX2-bound genes (ChIP-Seq) differentially expressed between control and $SOX2^{KO}$ cells (RNA-Seq), producing a set of 781 genes that were SOX2-bound and differentially expressed when SOX2 was deleted (Figure 4A). The majority of SOX2-bound genes had decreased expression upon SOX2 deletion (Figure 4B). Gene set enrichment analysis (GSEA) of RNA-Seq datasets demonstrate that SOX2 expression was significantly associated with several metabolic pathways, including oxidative phosphorylation, fatty acid metabolism, amino acid metabolism, and xenobiotic metabolism (Figure 4C). Further analyses of multiple gene sets associated with stem cell function were not significantly different (Supplemental Figure 2B). These data strongly prioritize a critical role for SOX2 in regulating multiple facets of cellular metabolism within prostate cancer cells.

GSEA Leading Edge analyses of SOX2-associated metabolic pathways prioritized a set of 28 genes that were SOX2-bound, differentially expressed between control and $SOX2^{KO}$ cells, and had multiple overlapping functions among significant metabolic GSEA pathways (Figure 4D). Additional analyses of data from Mu et al. whereby SOX2 expression increased as a result of RB/p53 depletion in LNCaP/AR prostate cancer cells also demonstrated notable changes in 10/28 of our prioritized genes (Figure 4E) [3]. We subsequently conducted further refinement and clinical validation of SOX2-associated regulation of genes involved in cellular metabolism by using publicly-available RNA-Seq datasets of human tissues. First, analyses of mRNA data from primary prostate tumors obtained via the TCGA PanCancer Atlas (n=494 patient tumors) demonstrated statistically significant correlations between SOX2 and metabolism-associated genes *CERK* (*ceramide kinase*), *ECHS1* (*enoyl-CoA hydratase, short chain 1*), *HS6ST1* (*heparan sulfate 6-O-sulfotransferase 1*), *LPCAT4* (*lysophosphatidylcholine acyltransferase 4*), *PFKP* (*phosphofructokinase, platelet*), *SLC16A3* (*solute carrier family 16 member 3*), *SLC46A3* (*solute carrier family 46 member 1*), and *TST* (*thiosulfate sulfurtransferase*) (Figure 4F) [30]. Second, analyses of RNA-Seq data comparing primary and metastatic tumors demonstrated statistically significant changes in expression among the same SOX2 gene targets *CERK*, *ECHS1*, *HS6SDT1*, *LPCAT4*, *PFKP*, *SLC16A3*, *SLC46A1*, and *TST* (Figure 4G) [31–33]. In both cases, directionality of expression matched our RNA-Seq data, whereby SOX2 expression was positivity correlated with *CERK*, *HS6ST1*, *LPCAT4*, *PFKP*, and *SLC16A3*, and SOX2 expression was negatively correlated with *ECHS1*, *SLC16A3*, and *TST* (Figure 4D–G). These data support a model whereby SOX2 expression, either within a primary tumor or acquired as a result of metastasis and therapy resistance, promotes a distinct cellular metabolism phenotype that is mediated by SOX2.

SOX2 Expression Promotes Increased Glycolysis, Oxidative Phosphorylation, and Mitochondrial Quantity

Prostate cancer metabolism deviates from the generally accepted Warburg phenotype, in that primary prostate cancer cells tend to rely on oxidative phosphorylation as the main energy source, while prostate cancer metastases shift toward a reliance on glycolysis for ATP production [34]. To define metabolic changes when SOX2 is lost (CWR-R1-$SOX2^{KO}$) or gained (LAPC4-SOX2; LAPC4 cells ectopically expressing lentiviral SOX2, termed

SOX2-OE), we measured and compared glycolysis and mitochondrial respiration between CWR-R1-control vs. CWR-R1-SOX2^{KO} and LAPC4-control vs. LAPC4-SOX2 cells. First, to measure glycolysis and glycolytic capacity, we used the Seahorse *Glycolysis Stress Test,* which measures key parameters of glycolytic flux such as glycolysis, glycolytic capacity, and glycolytic reserve. For both CWR-SOX2^{KO} and LAPC4-SOX2^{OE} cells, there was a significant SOX2-mediated correlation between glycolysis and glycolytic capacity, and for the LAPC4-SOX2^{OE} cells there was also a significant increase in glycolytic reserve (Figure 5A and B). In both cases, SOX2 expression was positively associated with elevated glycolytic activity compared to SOX2-negative cells. Furthermore, restoration of SOX2 expression in SOX2^{KO} cells via ectopic lentiviral re-expression of SOX2 (CWR-SOX2^{KO} + LV-SOX2) restored glycolytic activity back to those observed in the control group (Supplemental Figure 3). These data strongly support a model whereby SOX2 expression confers increased glycolytic activity in prostate cancer cells.

Second, to measure mitochondrial respiration, we used the Seahorse *Mitochondrial Stress Test*, whereby cells are treated with oligomycin to inhibit ATP synthase, and the decrease in oxygen consumption rate (OCR) provides a measurement of mitochondrial respiration associated with cellular ATP production. Subsequent injection of FCCP collapses the proton gradient and disrupts mitochondrial membrane potential, leading to uninhibited flow of electrons through the electron transport chain and maximal oxygen consumption by complex IV. The difference between the basal level of oxygen consumption and maximal oxygen consumption after FCCP treatment is deemed spare capacity, which measures the ability of a cell to respond to increased energy demand. These analyses demonstrated that SOX2-positive cells (CWR-R1-Control and LAPC4-SOX2^{OE} cells) had significantly increased basal respiration, maximal respiration, and spare respiratory capacity compared to SOX2-negative cells (CWR-R1-SOX2^{KO} and LAPC4-Control cells; Figure 5C and D). Additionally, restoration of SOX2 expression in SOX2^{KO} cells via ectopic lentiviral re-expression of SOX2 (CWR-SOX2^{KO} + LV-SOX2) restored maximal respiration and spare respiratory capacty back to those observed in the control group (Supplemental Figure 3).Thus, SOX2-expressing cells have a higher capacity for both mitochondrial respiration and glycolysis; this increase in metabolic capacity and energetic reserves could enable enhanced proliferation, therapy resistance, and plasticity of SOX2-positive prostate cancer cells.

To evaluate more global metabolic changes between SOX2-positive and SOX2-negative cells, we conducted metabolomic profiling of hydrophilic metabolites. These analyses demonstrated notable changes in purine metabolism, pyrimidine metabolism, amino acid and sugar metabolism, and the pentose phosphate pathway (PPP) that were significantly associated with SOX2 expression (Figure 5E). Further, there were no significant SOX2-associated changes in secreted citrate or lactate (CWR-R1-control vs. CWR-R1-SOX2^{KO}: citrate secretion, p=0.762; lactate secretion, p=0.146) (LAPC4-control vs. LAPC4-SOX2: citrate secretion, p=0.675; lactate secretion, p=0.125). With respect to changes in glycolysis, we noted significant changes in levels of fructose 6-phosphate/glucose 1-phosphate that were concordant with our Seahorse glycolysis data and changes in the SOX2 target PKFP among both CWR-R1 and LAPC4 cells (Figure 5F).

The observed SOX2-associated changes in mitochondrial respiration suggest that total mitochondria per cell may be impacted by SOX2 expression. PCR-based quantitation of total mitochondria demonstrated decreased total mitochondria in $SOX2^{KO}$ cells compared to controls and concordant increases total mitochondria in SOX2-OE cells compared to controls (Figure 5G). These data support a model whereby SOX2 mediates metabolic reprogramming of prostate cancer cells and elevated SOX2 expression, resulting in increased glycolysis, oxidative phosphorylation, and mitochondria quantity, thereby promoting increased metabolic production and cancer progression (Figure 5H).

DISCUSSION

Therapeutic resistance of prostate cancer is a significant clinical problem and the leading determinant in prostate cancer-associated mortalities. Thus, identification and characterization of new mechanisms and pharmacologic targets are critical to predict, prevent, and overcome cancer progression and therapy resistance. Here, we report that SOX2 expression in prostate tumors confers a poor patient prognosis and we mechanistically demonstrate that SOX2 directly mediates widespread changes in prostate cancer cell metabolism. These data prioritize SOX2 expression as an important functional and prognostic biomarker for prostate cancer and identify a cohort of transcriptional SOX2 targets that could be of therapeutic benefit.

Use of SOX2 as a prognostic biomarker in prostate cancer could significantly impact treatment decision-making practices and tumor staging. We previously showed that SOX2 expression is strikingly binary among prostate tumors, whereby tumors are either uniformly SOX2-positive or SOX2-negative [2]. Russo et al. and Matsika et al. further documented that SOX2 expression is associated with lymph node metastasis in prostate cancer [21, 35]. Using a robust and annotated set of tumor specimens with more than 20 years of patient follow-up, we demonstrated SOX2-associated increases in time to metastasis and decreased cancer-specific survival, supporting a model whereby SOX2 drives a more aggressive and therapy-resistant tumor phenotype. Interestingly, analyses also revealed a lack of association between SOX2 and PSA relapse after surgery (BCR). Increased PSA after local tumor therapy is suggestive of pending metastasis, although not all patients with detectable PSA after local therapy experience clinical recurrence or cancer-specific mortality [36, 37]. Our data suggest that SOX2 may be less critically involved in initial steps of cancer dissemination but rather functions to drive metastatic survival, growth, and therapy resistance and enable easier adaptation of disseminated tumor cells to their new metastatic microenvironment.

SOX2 is clearly implicated in promoting lineage plasticity in prostate cancer, and multiple groups demonstrated an association between expression of SOX2 and neuroendocrine genes with onset of the neuroendocrine prostate cancer (NEPC) cancer phenotype [38–43]. A role for SOX2 as an oncogene is further supported by multiple studies demonstrating SOX2-mediated changes in cell growth, invasion, and chemoresistance across multiple tumor types [6, 17, 44–48]. Further, we and others have shown that SOX2 is sufficient to enable castration-resistant tumor growth and resistance to the AR antagonist enzalutamide [2, 3]. The canonical role for SOX2 as an essential transcription factor for maintaining

and inducing embryonic stem cell pluripotency suggests that SOX2 expression in cancer confers a stem-like phenotype. Our data, however, demonstrate that the majority of SOX2-regulated gene targets in prostate cancer cells are non-overlapping with SOX2 targets in human embryonic stem cells, including differential SOX2 binding sites within what appear to be similar gene targets. This data also agrees with our previously published observation that SOX2 expression in prostate cancer cells was not associated with increased stem cell marker expression or sphere-forming ability [2]. These data suggest that SOX2 interacts with distinct, non-embryonic binding partners to regulate novel gene sets and carry out non-stem cell functions in adult cancer cells. However, the mechanisms and binding partners through which SOX2 confers these oncogenic phenotypes remain unclear, and continued delineation of SOX2-mediated oncogenic pathways is necessary to exploit SOX2 and its effector genes as therapeutic targets.

To date, there are few reports pertaining to a role for SOX2 in cancer metabolism [49]. Prostate cancer glucose metabolism uses a unique process, whereby primary prostate cancer cells tend to rely on oxidative phosphorylation as the main energy source and shift toward a reliance on glycolysis for ATP production during metastatic progression [50]. The metabolic profile of pluripotent embryonic stem cells is characterized by high glycolytic rates to support rapid cell proliferation, particularly during hypoxic conditions of the inner cell mass before embryo implantation [51]. There is substantial insight, however, into the metabolic changes and nutrient adaptation that cancer cells undergo during dissemination and metastatic colonization [52–54]. Such changes require metastatic cells to have adaptability and flexibility to change their metabolic requirements and nutrient utilization during metastatic progression. However, to date there is scant data supporting a direct, mechanistic link from SOX2 to mitochondria or glucose metabolism [27, 55]. Data presented here reveal unique and potentially novel opportunities to elucidate new mechanisms of SOX2 function in both embryonic and adult stem cells and to identify new approaches to pharmacologically target SOX2-dependent tumor cells. Additionally, SOX2-mediated changes in cancer cell metabolism may enable novel approaches to prostate cancer imaging, particularly positron emission tomography, to potentially detect SOX2-positive tumors [56, 57].

Our study provides a compelling argument for regulation of multiple aspects of prostate cancer cell metabolism by SOX2. Further, our findings are supported by clinical observations that SOX2 confers increased metastatic progression and poor patient overall survival. However, this study is not without limitations, and multiple opportunities for continued investigation are warranted. First, the paucity of clinically relevant human prostate cancer cell lines, particularly those expressing endogenous SOX2, limited our ability to investigate SOX2 function throughout cancer initiation and progression. Future use of patient-derived xenograft models and 3D organoid model systems will be instrumental in precisely defining the function of SOX2 during distinct stages of cancer progression. Second, we cannot exclude the contribution of downstream molecular events resulting from SOX2 deletion or over-expression. Given the scope and quantity of the SOX2 target genes identified, multiple additional pathways likely contribute to our observed in vitro and in vivo phenotypes beyond cellular metabolism. Third, annotated patient specimens represent a retrospective cohort of patients who underwent an array of evolving treatment and imaging

modalities over 20 years of follow-up. The biomarker utility of SOX2-associated differences to predict metastases and survival should be optimally tested via a large prospective study given the potential prognostic value of SOX2 expression.

Conclusion:

Tumor SOX2 expression is associated with poor patient prognosis and a higher likelihood of prostate cancer-specific death. Within prostate cancer cells, SOX2 regulates genes promoting metabolic reprogramming by increasing mitochondrial quantity, glycolysis, and oxidative phosphorylation. Further, many SOX2-regulated genes are not stem cell-related genes and are potentially unique to prostate cancer cells. These data highlight new and critical avenues of future investigation and clinical analyses to exploit SOX2 oncogenic dependencies for patient benefit.

METHODS

Cell Lines and Materials

R1881 was purchased from Sigma-Aldrich (St. Louis, MO) and stored at −20°C in ethanol. Human prostate cancer cell lines were grown as previously described [2, 58]. Cell authentication of all cells was confirmed via The University of Arizona Genetics lab (Tucson, AZ). All cultures were routinely screened for the absence of mycoplasma contamination using the ATCC Universal Mycoplasma Detection Kit (Manassas, VA). LAPC4 cells were grown in IMDM (Hyclone; Logan, UT) supplemented with 1% penicillin/streptomycin (Corning; Corning, NY), 10% fetal bovine serum (Atlanta Biologicals; Flowery Branch, GA), and 1 nM R1881 (Sigma-Aldrich; St. Louis, MO). CWR-R1 cells were grown in RPMI-1640 (Gibco, Thermo Fisher Scientific; Waltham, MA) supplemented with 1% penicillin/streptomycin (Corning) and 10% fetal bovine serum (Atlanta Biologicals). Lentiviral SOX2 (LV-SOX2) was obtained from Vector Builder (Hygromycin-resistance, CMV promoter; Chicago, IL). For enzalutamide treatment, 10 μM enzalutamide (Selleck Chemical; Houston, TX) was added in media with 10% charcoal-stripped fetal bovine serum (Atlanta Biologicals). For all experiments, equimolar vehicle (DMSO) was added. The human embryonic stem cell (hESC) line WA01(H1) was acquired from WiCell (Madison, WI) and cultured using the feeder-independent protocol in mTeSR1 media (Stem Cell Technologies; Vancouver, B.C.). hESCs were used within ten passages of thawing and were dissociated using mTeSR1 media with Accutase (Millipore; Billerica, MA) digestion.

Human Subjects and Tissue Microarrays (TMAs)

All human tissues were acquired under an expedited protocol approved and monitored by the University of Chicago Institutional Review Board. We acquired the 726-case PSA progression TMA from the Prostate Cancer Biorepository Network (PCBN; http://prostatebiorepository.org; Supplemental Table 1) [23, 24]. This nested case-control study was designed specifically to evaluate biomarkers for prostate cancer recurrence, beyond known prognostic factors (age at surgery, race, pathologic stage, and Gleason sum in prostatectomy specimen) [23, 24]; specimens and data was obtained with informed consent. The full nested case-control study includes 524 recurrence cases and a sample of 524

controls identified among 4,860 prostate cancer patients who underwent radical retropubic prostatectomy for clinically localized prostate cancer at Johns Hopkins in Baltimore, MD during 1993 –2001. The dataset of 1,048 records (524 matched pairs) includes 742 unique men, with some men serving as controls for multiple cases, and some men who were controls were later sampled as cases. The sample does not include men who received hormonal or radiation therapy before their prostatectomy or hormonal adjuvant therapy before recurrence. These men were followed for outcome through 2004. Recurrence was defined as biochemical recurrence (BCR, serum PSA >0.2 ng/mL), local recurrence, systemic metastases, or death from prostate cancer. For each case, incidence density sampling [59] was used to select a control who had not experienced recurrence by the date of the case's recurrence and who was similar to the case in age at surgery, race, pathologic stage, and Gleason sum in the prostatectomy specimen. The TMA contained four cores each of normal and cancerous tissues per patient.

Tissues were analyzed by a trained and blinded genitourinary pathologist and scored on percentage of cells with positive nuclear staining (0 = no staining; 1 = 1%–5% positive cells; 2 = 5%–50% positive cells; and 3 = 50%–100% positive cells). Patients were divided into two groups for analysis: patients with a composite score of 0–1 were considered SOX2-negative, whereas patients with a score ≥2 were considered SOX2-positive. For images, slides were digitized using a Pannoramic Scan whole slide scanner (Cambridge Research and Instrumentation; Hopkinton, MA) and images captured using Pannoramic Viewer software version 1.14.50 (3DHistech; Budapest, Hungary).

Histology and Immunostaining

Hematoxylin and eosin staining was performed as previously described using a Sakura Tissue-Tek Prima Autostainer (Torrance, CA) [2]. For IHC staining, formalin-fixed, paraffin-embedded slides were deparaffinized in xylene and hydrated using graded ethanol washes. Tissues were treated with antigen retrieval buffer (S1699 from DAKO; Glostrup, Denmark) in a steamer for 20 min. Anti-SOX2 (D6D9 rabbit monoclonal, Cell Signaling Technology; Danvers, MA) was applied for 1 h at room temperature in a humidity chamber. Following TBS wash, antigen–antibody binding was detected with Envision+system (K4001, DAKO; Carpinteria, CA) and DAB+Chromogen (K3468, DAKO). Tissue sections were briefly immersed in hematoxylin for counterstaining and were cover-slipped. Staining quantitation was conducted by a genitourinary pathologist. Controls for specificity of anti-SOX2 staining using the D6D9 antibody are shown in Supplemental Figure 1.

In Vivo Tumor Xenografting

Inoculation and growth of human xenograft tumors was conducted as previously described [60]. All mice used in this study were 4–6-week-old male athymic nude mice (Harlan; Indianapolis, IN). All animal studies were carried out in strict accordance with recommendations in the Guide for the Care and Use of Laboratory Animals of the National Institutes of Health. The protocol was approved by the University of Illinois at Chicago IACUC. Mice were castrated, and half were given 1 cm silastic testosterone implants to stabilize host hormone levels [60, 61]. One million cells were prepared in a mixture of 75% Matrigel and 25% PBS and injected into the flanks of nude mice. No randomization

or blinding was utilized. Tumor formation and growth were monitored using caliper measurements.

Quantitative Real-Time PCR Analyses

RNA was purified using the Qiagen RNeasy Mini Kit with optional DNAse digestion kit (Qiagen; Valencia, CA) and quality tested using an Agilent Bioanalyzer 2100 (Agilent Technologies; Santa Clara, CA). For standard Q-RT-PCR, extracted RNA was converted to cDNA by reverse transcription using SuperScript III Reverse Transcriptase (Invitrogen; Carlsbad, CA). Expression levels of *SOX2* and *RPL13A* transcript were quantified using Power SYBR Green Master Mix (Invitrogen) using custom primers: *SOX2* (forward 5'-GCGGAAAACCAAGACGCTC-3'; reverse 5'-TCAGCGCGTAACTGTCC-3'), *RPL13A* (forward 5'-GGAGCAAGGAAAGGGTCTTAG-3'; reverse 5'-GGTTGCTCTTCCTATTGGTCATA-3'). Standard curves were used to assess primer efficiency, and average change in threshold cycle (ΔCT) values was determined for each sample relative to endogenous *RPL13A* levels and compared to vehicle control (ΔΔCT). Experiments were performed in triplicate to determine mean standard error, and student's t-tests were performed with normalization to control to obtain p-values.

Mitochondria levels were quantified with qPCR of genomic DNA using two mtDNA primer sets [$tRNA^{Leu(UUR)}$ and 16S rRNA] and one nuclear DNA primer set (β2-microglobulin) (Reference [62], Supplement 68, 19.7.4; qPCR Analysis of mtDNA Content). Primer sets were: tRNA F3212 5'-CACCCAAGAACAGGGTTTGT-3'; tRNA R3319 5'-TGGCCATGGGTATGTTGTTA-3'; mtF3162 5'GCCTTCCCCCGTAAATGATA-3'; mtR3260 5'-TTATGCGATTACCGGGCTCT-3'; β2M F594 5'-TGCTGTCTCCATGTTTGATGTATCT-3'; β2M R679 5'-TCTCTGCTCCCCACCTCTAAGT-3'.

Western Blotting

Whole-cell lysates of ≥100,000 cells were used per lane. Western blotting was performed as previously reported [2]. Briefly, cells were rinsed with cold PBS and scraped into RIPA buffer supplemented with protease inhibitors, sonicated twice, and re-suspended in 4X sample buffer (BioRad; Hercules, CA) supplemented with 10% beta-mercaptoethanol (Sigma-Aldrich; St. Louis MO). The Pierce BCA protein assay kit (Thermo Fisher Scientific; Grand Island, NY) was used to determine protein concentration. Protein (60 μg) was electrophoresed on 10% SDS-polyacrylamide gels and transferred to nitrocellulose (Odyssey, LI-COR Biosciences; Lincoln, NE) overnight at 4°C. Membranes were blocked overnight in 5% non-fat milk in TBS at 4°C. Primary antibodies used were: anti-SOX2 (D6D9 rabbit monoclonal, Cell Signaling Technologies) and anti-beta actin (clone AC-15, Sigma-Aldrich). Secondary antibodies were goat anti-mouse IRDye 800 CW or donkey anti-rabbit IRDye 680 (LI-COR Biosciences), and images were captured using an infrared Odyssey scanner (LI-COR Biosciences).

CRISPR-Cas9 Targeting to Block *SOX2* Expression

To generate CRISPR/Cas9-mediated $SOX2^{KO}$ cell lines, parental CWR-R1 cells were co-transfected with pT2-EF1a-Cas9-P2A-puro and pCMV(CAT)T7-SB100 (#34879, Addgene;

Watertown, MA) using Lipofectamine 2000 (Invitrogen) to introduce Cas9 expression. Stable constitutive Cas9 expression was accomplished by SB100 transposase integration of EF1a-Cas9-P2A-puro. Cas9-expressing cells were selected for and maintained with puromycin (1 mg/mL, Invitrogen) 48 h after transfection. Constitutive Cas9 expression was confirmed by western blot (# 14697, Cell Signaling Technologies) after 1 week of puromycin selection. Two custom crRNAs (Integrated DNA Technologies; Coralville, IA) targeting the N-terminus of SOX2 were selected using CHOPCHOP software (https://chopchop.cbu.uib.no) (SOX2 crRNA #1: 5'-CGGGCCCGCAGCAAACTTCG-3', SOX2 crRNA #2: 5'-CGCCCGCATGTACAACATGA-3') and were individually complexed with tracrRNA-ATTO 550 (#1075927, Integrated DNA Technologies) at a 1:1 ratio immediately before transfection. A final concentration of 10 nM crRNA:tracrRNA duplexes were transfected into CWRR1-Cas9 cells using siLentFect Lipid Reagent for RNAi (#1703360, BioRad) following manufacturer guidelines. Limited dilution was performed to isolate three clonal knockout cell lines, and successful knockout of SOX2 was validated by western blot (anti-SOX2(D6D9), #3579, Cell Signaling Technologies).

ChIP-Seq and RNA-Seq

SOX2 ChIP-Seq: CWR-R1 and WA01 cells were cultured as described above, and methods for ChIP were adapted from previously reported methods [63]. DNA and associated proteins were crosslinked with 1% formaldehyde, and lysates were sonicated and immunoprecipitated as described previously [2]. ChIP experiments were conducted using the ChIP Assay Kit per the manufacturer's protocol (EMD Millipore; Burlington, MA). A polyclonal goat anti-SOX2 mAb (P48431, R&D Systems; Minneapolis, MN) or goat IgG control were used for immunoprecipitation. Eluted ChIP DNA was purified using the PCR Purification Kit (Qiagen). ChIP-Seq libraries were generated using the KAPA LTP Library Preparation Kit (#KK8230; Kapa Biosystems; Wilmington, MA). Libraries were sequenced on a HiSeq 2000 sequencing system (Illumina) in a 50-bp, single-end run.

RNA-Seq: RNA was purified using the RNeasy Mini Kit (Qiagen). RNA quality was evaluated using a 2200 TapeStation system (Agilent), and samples with RNA integrity score score ≥ 7 were selected for library preparation. RNA-Seq libraries were prepared and amplified according to KAPA Stranded mRNA-Seq Kit-Illumina Platforms (KAPA Biosystems), using Oligo-dT magnetic beads to enrich for mRNA. Sample library fragment sizes were confirmed using a 2200 TapeStation system (Agilent) and quantified by qPCR using the Library Quantification kit (KAPA Biosystems). Library adaptors 1–12 (KAPA Biosystems) were used to barcode each sample, and libraries were sequenced on a HiSeq 2000 sequencing system (Illumina) in a 100-bp, paired-end run.

Datasets: ChIP-Seq and RNA-Seq datasets are deposited in NCBI Gene Expression Omnibus (GEO) under the accession number GSE166185.

Analyses of Sequencing Data

ChIP-Seq Peak and Region Analysis: All ChIP-Seq reads were analyzed using the FastQC tool suite (http://www.bioinformatics.babraham.ac.uk/projects/fastqc). Low-quality and adapter sequences were trimmed using Trimmomatic [64]. Trimmed reads were then

aligned to the reference genome GRCh38 using BWA [65], and resulting alignments were sorted and converted to BAM format using Samtools (http://www.htslib.org/doc/samtools.html). Duplicate reads were subsequently removed with Picard tools (http://broadinstitute.github.io/picard). MACS2 [66] was used for peak detection for SOX2 immunoprecipitation data. Peak images were captured using Integrative Genomics Viewer (http://software.broadinstitute.org/software/igv).

Transcription Factor Motif Analysis: SOX2 peak regions that passed selection criteria were expanded to a uniform range of 250 bp around the summit to submit targeted sequences for motif analysis using MEME Suite [67]. In addition, FIMO [68] was used to scan for all JASPAR (vertebrates 2016) transcription factor motifs [69]. In the set of SOX2 peaks where a canonical SOX2 motif was discovered, SpaMo was used to infer potential binding partners.

RNA-Seq Differential Expression: All RNA-Seq reads were analyzed using the FastQC tool suite. Low-quality and adapter sequences were trimmed using trimmomatic [64]. Trimmed reads were aligned to the reference genome GRCh38 using STAR, and resulting alignments were sorted and converted to BAM format using Samtools. Duplicate reads were subsequently removed with Picard tools. Differentially expressed genes (DEGs) were detected using featureCounts-DESeq2 or EdgeR (read count-based method). Transcripts were further filtered by fold change ≥1.5. Biological insights from candidate gene lists were gained by performing GSEA and IPA (Ingenuity Systems, Qiagen) to identify significantly altered functional categories or pathways. Heatmaps were generated using the Morpheus platform (https://software.broadinstitute.org/morpheus).

Analysis of Publicly-Available RNA-Seq Datasets

We obtained raw RNA-Seq FASTQ files of 25 prostate tumors, three benign glands, and 51 annotated metastases via dbGAP (phs000310.v1.p1 for tumors and benign glands; phs000915.v1.p1 for metastases) [31–33]. These datasets were chosen based upon mRNA quality, sequencing depth, and annotation. Tumor datasets are from patients who underwent prostate surgery without prior therapy, and metastases are from patients with castration-resistant prostate cancer, some of which had received taxane, enzalutamide, or abiraterone treatment [32, 33]. Quality of raw reads was accessed by FastQC (v0.11.4). All reads were mapped to the human genome assembly (NCBI build 19) using STAR (v2.5.1b). Alignment metrics were collected by Picard tools (v2.8.1) and RSeQC (v2.6.4) [70]. Transcripts were assembled from aligned reads using Cufflinks and combined with known gene annotation. The expression level of transcripts was quantified using FPKM-based and read count-based methods. Transcript expression was normalized across samples. Multiple gene expression correlations were determined using the cBioPortal for Cancer Genomics (www.cbioportal.org) using The Cancer Genome Atlas Prostate Adenocarcinoma [30] dataset consisting of 333 samples with annotated mRNA expression z-scores.

Cell Proliferation Assays

Cell Growth Assay: Cells with nuclear GFP were plated at a density of 10,000 cells per well in a 96-well plate, followed by the indicated treatment the following day. Wells were

placed in the IncuCyte S3 Live Cell Analysis System (Essen Bioscience, Ann Arbor, MI) and imaged every 4 h for 120 h. Cell number was counted for each image using built-in analysis software. Cell numbers per subsequent time point were normalized to initial number of cells (time 0). All assays were repeated at least three times.

BrdU Assay: Cells were treated for 72 h with enzalutamide and were ~70% confluent when they were pulsed with 30 μM BrdU for 2 h. Cells were fixed with 70% ethanol for 30 min, and DNA was denatured using 2 N hydrochloric acid/0.5% Triton X-100 for 30 min. Anti-BrdU-FITC antibody solution (#11–5071-42, 1:20 dilution, Thermo Fisher Scientific) was added for 1 h. DNA was stained with a propidium iodide solution (#40017, 1:20 dilution, Biotium; Hayward, CA) supplemented with RNase A (#EN0531, 1:100 dilution, Thermo Fisher Scientific) overnight at 4°C. Cells were analyzed by flow cytometry (Gallios Bench-top Analyzer, Beckman Coulter; Brea, CA).

Apoptosis Assays

Propidium Iodide Exclusion Assay: In 6-well plates, 150,000 cells were plated and allowed to attach overnight. Cells were treated with vehicle and 10 μM enzalutamide for 72 h. Propidium iodide (#40017, Biotium) was added to each well at a concentration of 1 μg/mL and incubated for 15 min at 37°C. Supernatant was collected as well as trypsinized cells. Propidium iodide-positive cells (non-viable cells) were counted using Cellometer Spectrum (Nexcelom Bioscience; Lawrence, MA).

RealTime-Glo Annexin V Apoptosis and Necrosis Assay: In solid white-bottom 96-well plates (#353296, Corning), 10,000 cells were plated and allowed to attach overnight. Cells were treated with vehicle, 10 μM enzalutamide, or 2 mM staurospaurine (positive control) in triplicate, and RealTime-Glo Annexin V Apoptosis and Necrosis kit (#JA1011, Promega; Madison, WI) was added per manufacturer instructions. Briefly, 50 μL containing 10,000 cells were added to each well of a 96-well plate. The next day, 50 μL of 4X concentrated drugs (vehicle, enzalutamide, or staurospaurine) and 100 μL of 2X detection reagents were added. Luminescence and fluorescence (485 nm/525 nm) were measured daily using the Synergy LX Multimode Reader (Biotek; Winooski, VT) and normalized to blank wells.

TUNEL Assay: In black, clear-bottom plates (#3603, Corning), 5,000 cells were plated and allowed to attach overnight. Cells were treated for 72 h with vehicle or 10 μM enzalutamide. Cells were processed as per the manual for Click-iT TUNEL Alexa Fluor 647 Imaging Assay (#C10247, Thermo Fisher Scientific). Briefly, cells were fixed with 4% paraformaldehyde and permeabilized with 0.25% Triton X-100 in PBS. DNAse I (included in the kit) was used to generate strand breaks in the DNA as a positive control. TdT reaction cocktail was added to each well and was followed by the Click-iT reaction cocktail. Each well was imaged using the Keyence BZ-X800 microscope (Keyence; Osaka, Japan).

Cellular Metabolism Assays

To determine cell energetics as well as glycolysis and oxidative phosphorylation rates, cells were seeded at a density of 50,000 cells per well. Cells were counted and plated in

Seahorse Xfe24 plates (Agilent) 24 h before assay and allowed to attach overnight. The assay cartridge was hydrated with Agilent equilibration buffer in a 0% CO_2 chamber at 37°C overnight. One hour before assay, culture media was removed and replaced with Seahorse assay media (Seahorse basal RPMI media supplemented with 2 mM L-glutamine and 11 mM glucose for Cell Mito Stress Test). Extracellular acidification rate (ECAR) and oxygen consumption rate (OCR) were measured using the Agilent Seahorse Xfe24 machine, according to manufacturer instructions for the Glycolysis Stress Test and Cell Mito Stress Test. FCCP and oligomycin from Cell Energy Phenotype Test kit were used with rotenone (#3616, Tocris Bioscience; Bristol, UK), 2-DG (#B1048–500, Biovision Inc.; Milpitas, CA), and antimycin A (#SC-202467A, Santa Cruz Biotechnology; Dallas, TX). Assays were analyzed using Seahorse Wave Software (Agilent). Cell density and concentration of FCCP (1 μM) were optimized according to manufacturer's instructions.

Metabolite Secretion Assay and Analysis

Cells were plated in fresh media and incubated for 48 h. Protein quantification was performed using proxy wells for normalization. Norvaline was used as an internal standard. Citrate and lactate standards were used to generate a standard curve for quantification. Metabolite extraction was performed using HPLC-grade ethanol (Sigma Aldrich). Samples were derivatized with methoxamine (PI45950, Thermo Fisher Scientific) and *N*-*tert*-butyldimethylsilyl-*N*-methyltrifluoroacetamide with 1% *tert*-butyldimethylchlorosilane (Sigma Aldrich). Samples were analyzed by GC/MS using a HP-5MS Ultra Inert GC column (19091S-433UI, Agilent Technologies) installed in an Agilent 7890B gas chromatograph coupled to an Agilent 5977B mass spectrometer. Helium was used as the carrier gas. One microliter of sample was injected at 280°C. After injection, the GC oven was held at 60°C for 1 min. The oven ramped up to 320°C at 10°C/min and held for 9 min. The MS system operated under electron impact ionization mode at 70 eV, and the MS source and quadrupole were held at 230°C and 150°C, respectively. Peak abundance was determined by automated integration using MassHunter software (Agilent). Total abundance was normalized to the norvaline internal standard. Secretion rate was calculated by taking into account the specific growth rate, as determined by pre- and post-assay protein quantification.

Metabolite Analysis

Samples were prepared according to the protocol from Northwestern University's Metabolomics Core Facility (https://nucore.northwestern.edu/facilities/Metabo). Briefly, cells were grown in 10 cm dishes until reaching 60%–80% confluency. Media was changed 2 h before starting cell preparation, where cells were washed twice with ice-cold saline (not PBS), and 1 mL of ice-cold 80% methanol was added. Cells were incubated at −80°C for 20 min, scraped into Eppendorf tubes, and subjected to three freeze-thaw cycles between –80°C and 37°C, vortexing 30 s after each thaw. Samples were centrifuged for 15 min at 4°C at >15,000 rcf, and supernatant was transferred to new tubes. Samples were dried using Speedvac at the Metabolomics facility. Total protein quantification was performed as described above to normalize metabolites for injection.

Cell Migration Assays

Cells were treated for the indicated number of days with vehicle or enzalutamide and were serum-starved 24 h before plating for migration assays. Cells were plated at 200,000 cells per well into transparent PET membrane inserts (24-well, 8.0-μm pore size, Corning) in serum-free conditions with the indicated treatments. Wells outside of inserts contained media with serum and the indicated treatments. Aphidicolin (Cayman Chemical; Ann Arbor, MI) was added as a proliferation inhibitor. Membranes were fixed and stained 48 h post-plating with a crystal-violet solution, mounted, and imaged using the Keyence BZ-X800 All-in-one fluorescence microscope. The numbers of cells migrated were counted using ImageJ.

Statistical Analyses

For tissue analyses, descriptive statistics of all variables are summarized for BCR and control patients (Supplemental Table 1). Two-sided t tests were used to compare continuous variables, and chi-square tests were used to compare categorical variables between BCR and control groups. All statistical analyses used SAS software with significance levels of 0.05. Post-operative outcomes between patients bearing SOX2-positive and -negative tumors were analyzed using Chi-square tests. Cox proportional-hazards model was used to analyze association between SOX2-positive to metastasis risk.

For phenotypic analyses, Tukey's multiple comparisons test was used for the growth curves, cell cycle, BrdU, propidium iodide exclusion, apoptosis, and TUNEL assays to compare all conditions. For Seahorse assays, Mann-Whitney test was used to compare control cells to $SOX2^{KO}$ cells.

Supplementary Material

Refer to Web version on PubMed Central for supplementary material.

ACKNOWLEDGEMENTS

We acknowledge Vander Griend and Szmulewitz lab members for their input; Dr. Brendan Looyenga at Calvin College for his gift of vectors used to generate knockout cell lines using CRISPR; support of the University of Illinois at Chicago Department of Pathology led by Dr. Fred Behm, as well as the University of Illinois at Chicago Research Histology and Tissue Imaging Core led by Dr. Peter Gann; Drs. Bruce Trock and Karen Sfanos of the Prostate Cancer Biorepository Network (PCBN) for help obtaining annotated tumor specimens and data; expert technical assistance of the Human Tissue Resource Center core facility led by Dr. Mark Lingen, and the assistance of Mary Jo Fekete; the Immunohistochemistry Core Facility run by Terri Li; the Northwestern University Metabolomics Core Facility for their assistance and service; the University of Chicago Genomics Facility led by Dr. Pieter Faber; support of the University of Chicago Committee on Cancer Biology, led by Dr. Kay Macleod and Stephen Kron; and support of Drs. Alan Diamond, Larisa Nonn, and Gail Prins at the University of Illinois at Chicago Departments of Pathology and Urology.

Funding:

R01CA178431 (DJ Vander Griend), R00CA218885-04 (P.M.); University of Chicago Comprehensive Cancer Center Support Grant (P30CA014599); The Brinson Foundation; Alvin Baum Family Fund; The Pierce Foundation; and National Center for Advancing Translational Sciences (UL1TR002003). The Prostate Cancer Biorepository Network is funded by the Department of Defense Prostate Cancer Research Program Award No. W81XWH-14-2-0182, W81XWH-14-2-0183, W81XWH-14-2-0185, W81XWH-14-2-0186, and W81XWH-15-2-0062, and W81XWH-18-1-0411 (P.M.). L. de Wet was supported by the Goldblatt Foundation

Fellowship; S. Kregel was supported by a Cancer Biology Training Grant (T32 CA 009594). P.M. is also supported by CPRIT (RR170050), Welch Foundation (I-2005-20190330) and Prostate Cancer Foundation (17YOUN12).

REFERENCES CITED

1. Ku SY, Rosario S, Wang Y, Mu P, Seshadri M, Goodrich ZW et al. Rb1 and Trp53 cooperate to suppress prostate cancer lineage plasticity, metastasis, and antiandrogen resistance. Science 2017; 355: 78–83. [PubMed: 28059767]
2. Kregel S, Kiriluk KJ, Rosen AM, Cai Y, Reyes EE, Otto KB et al. Sox2 is an androgen receptor-repressed gene that promotes castration-resistant prostate cancer. PloS one 2013; 8: e53701. [PubMed: 23326489]
3. Mu P, Zhang Z, Benelli M, Karthaus WR, Hoover E, Chen CC et al. SOX2 promotes lineage plasticity and antiandrogen resistance in TP53- and RB1-deficient prostate cancer. Science 2017; 355: 84–88. [PubMed: 28059768]
4. Zhang S, Cui W. Sox2, a key factor in the regulation of pluripotency and neural differentiation. World journal of stem cells 2014; 6: 305. [PubMed: 25126380]
5. Wegner M All purpose Sox: The many roles of Sox proteins in gene expression. The international journal of biochemistry & cell biology 2010; 42: 381–390. [PubMed: 19631281]
6. Stolzenburg S, Rots MG, Beltran AS, Rivenbark AG, Yuan X, Qian H et al. Targeted silencing of the oncogenic transcription factor SOX2 in breast cancer. Oxford University Press, 2012.
7. Ji J, Zheng P-S. Expression of Sox2 in human cervical carcinogenesis. Human pathology 2010; 41: 1438–1447. [PubMed: 20709360]
8. Jia X, Li X, Xu Y, Zhang S, Mou W, Liu Y et al. SOX2 promotes tumorigenesis and increases the anti-apoptotic property of human prostate cancer cell. Journal of molecular cell biology 2011; 3: 230–238. [PubMed: 21415100]
9. Hütz K, Mejías-Luque R, Farsakova K, Ogris M, Krebs S, Anton M et al. The stem cell factor SOX2 regulates the tumorigenic potential in human gastric cancer cells. Carcinogenesis 2013; 35: 942–950. [PubMed: 24325912]
10. Chen S, Li X, Lu D, Xu Y, Mou W, Wang L et al. SOX2 regulates apoptosis through MAP4K4-survivin signaling pathway in human lung cancer cells. Carcinogenesis 2013; 35: 613–623. [PubMed: 24233838]
11. Alonso MM, Diez-Valle R, Manterola L, Rubio A, Liu D, Cortes-Santiago N et al. Genetic and epigenetic modifications of Sox2 contribute to the invasive phenotype of malignant gliomas. PloS one 2011; 6: e26740. [PubMed: 22069467]
12. Han X, Fang X, Lou X, Hua D, Ding W, Foltz G et al. Silencing SOX2 induced mesenchymal-epithelial transition and its expression predicts liver and lymph node metastasis of CRC patients. PloS one 2012; 7: e41335. [PubMed: 22912670]
13. Sun C, Sun L, Li Y, Kang X, Zhang S, Liu Y. Sox2 expression predicts poor survival of hepatocellular carcinoma patients and it promotes liver cancer cell invasion by activating Slug. Medical Oncology 2013; 30: 503. [PubMed: 23430442]
14. Lou X, Han X, Jin C, Tian W, Yu W, Ding D et al. SOX2 targets fibronectin 1 to promote cell migration and invasion in ovarian cancer: new molecular leads for therapeutic intervention. Omics: a journal of integrative biology 2013; 17: 510–518. [PubMed: 23895273]
15. Bareiss PM, Paczulla A, Wang H, Schairer R, Wiehr S, Kohlhofer U et al. SOX2 expression associates with stem cell state in human ovarian carcinoma. Cancer research 2013; 73: 5544–5555. [PubMed: 23867475]
16. Chen S, Xu Y, Chen Y, Li X, Mou W, Wang L et al. SOX2 gene regulates the transcriptional network of oncogenes and affects tumorigenesis of human lung cancer cells. PloS one 2012; 7: e36326. [PubMed: 22615765]
17. Herreros-Villanueva M, Zhang J, Koenig A, Abel E, Smyrk TC, Bamlet W et al. SOX2 promotes dedifferentiation and imparts stem cell-like features to pancreatic cancer cells. Oncogenesis 2013; 2: e61. [PubMed: 23917223]
18. Vazquez-Martin A, Cufí S, Lopez-Bonet E, Corominas-Faja B, Cuyàs E, Vellon L et al. Reprogramming of non-genomic estrogen signaling by the stemness factor SOX2 enhances the

tumor-initiating capacity of breast cancer cells. Cell Cycle 2013; 12: 3471–3477. [PubMed: 24107627]

19. Yu X, Cates JM, Morrissey C, You C, Grabowska MM, Zhang J et al. SOX2 expression in the developing, adult, as well as, diseased prostate. Prostate Cancer Prostatic Dis 2014; 17: 301–309. [PubMed: 25091041]
20. Ugolkov AV, Eisengart LJ, Luan C, Yang XJ. Expression analysis of putative stem cell markers in human benign and malignant prostate. Prostate 2011; 71: 18–25. [PubMed: 20583131]
21. Matsika A, Srinivasan B, Day C, Mader SA, Kiernan DM, Broomfield A et al. Cancer stem cell markers in prostate cancer: an immunohistochemical study of ALDH1, SOX2 and EZH2. Pathology 2015; 47: 622–628. [PubMed: 26517640]
22. Russo MV, Esposito S, Tupone MG, Manzoli L, Airoldi I, Pompa P et al. SOX2 boosts major tumor progression genes in prostate cancer and is a functional biomarker of lymph node metastasis. Oncotarget 2016; 7: 12372–12385. [PubMed: 26540632]
23. Hempel HA, Cuka NS, Kulac I, Barber JR, Cornish TC, Platz EA et al. Low Intratumoral Mast Cells Are Associated With a Higher Risk of Prostate Cancer Recurrence. Prostate 2017; 77: 412–424. [PubMed: 27868214]
24. Toubaji A, Albadine R, Meeker AK, Isaacs WB, Lotan T, Haffner MC et al. Increased gene copy number of ERG on chromosome 21 but not TMPRSS2-ERG fusion predicts outcome in prostatic adenocarcinomas. Mod Pathol 2011; 24: 1511–1520. [PubMed: 21743434]
25. McAuley E, Moline D, VanOpstall C, Lamperis S, Brown R, Vander Griend DJ. Sox2 Expression Marks Castration-Resistant Progenitor Cells in the Adult Murine Prostate. Stem Cells 2019; 37: 690–700. [PubMed: 30720908]
26. Boyer LA, Lee TI, Cole MF, Johnstone SE, Levine SS, Zucker JP et al. Core transcriptional regulatory circuitry in human embryonic stem cells. Cell 2005; 122: 947–956. [PubMed: 16153702]
27. Sarkar A, Hochedlinger K. The sox family of transcription factors: versatile regulators of stem and progenitor cell fate. Cell Stem Cell 2013; 12: 15–30. [PubMed: 23290134]
28. Liu P, Sanalkumar R, Bresnick EH, Keleş S, Dewey CN. Integrative analysis with ChIP-seq advances the limits of transcript quantification from RNA-seq. Genome research 2016; 26: 1124–1133. [PubMed: 27405803]
29. Antonarakis ES, Lu C, Wang H, Luber B, Nakazawa M, Roeser JC et al. AR-V7 and resistance to enzalutamide and abiraterone in prostate cancer. N Engl J Med 2014; 371: 1028–1038. [PubMed: 25184630]
30. Cancer Genome Atlas Research N. The Molecular Taxonomy of Primary Prostate Cancer. Cell 2015; 163: 1011–1025. [PubMed: 26544944]
31. Bhanvadia RR, VanOpstall C, Brechka H, Barashi NS, Gillard M, McAuley EM et al. MEIS1 and MEIS2 Expression and Prostate Cancer Progression: A Role For HOXB13 Binding Partners in Metastatic Disease. Clin Cancer Res 2018; 24: 3668–3680. [PubMed: 29716922]
32. Pflueger D, Terry S, Sboner A, Habegger L, Esgueva R, Lin PC et al. Discovery of non-ETS gene fusions in human prostate cancer using next-generation RNA sequencing. Genome Res 2011; 21: 56–67. [PubMed: 21036922]
33. Robinson D, Van Allen EM, Wu YM, Schultz N, Lonigro RJ, Mosquera JM et al. Integrative clinical genomics of advanced prostate cancer. Cell 2015; 161: 1215–1228. [PubMed: 26000489]
34. Cutruzzolà F, Giardina G, Marani M, Macone A, Paiardini A, Rinaldo S et al. Glucose metabolism in the progression of prostate cancer. Frontiers in physiology 2017; 8: 97. [PubMed: 28270771]
35. Russo MV, Esposito S, Tupone MG, Manzoli L, Airoldi I, Pompa P et al. SOX2 boosts major tumor progression genes in prostate cancer and is a functional biomarker of lymph node metastasis. Oncotarget 2016; 7: 12372. [PubMed: 26540632]
36. Lowrance WT, Breau RH, Chou R, Chapin BF, Crispino T, Dreicer R et al. Advanced Prostate Cancer: AUA/ASTRO/SUO Guideline PART I. J Urol 2021; 205: 14–21. [PubMed: 32960679]
37. Van den Broeck T, van den Bergh RCN, Arfi N, Gross T, Moris L, Briers E et al. Prognostic Value of Biochemical Recurrence Following Treatment with Curative Intent for Prostate Cancer: A Systematic Review. Eur Urol 2019; 75: 967–987. [PubMed: 30342843]

38. Metz EP, Wilder PJ, Dong J, Datta K, Rizzino A. Elevating SOX2 in prostate tumor cells upregulates expression of neuroendocrine genes, but does not reduce the inhibitory effects of enzalutamide. J Cell Physiol 2020; 235: 3731–3740. [PubMed: 31587305]
39. Li H, Wang L, Li Z, Geng X, Li M, Tang Q et al. SOX2 has dual functions as a regulator in the progression of neuroendocrine prostate cancer. Lab Invest 2020; 100: 570–582. [PubMed: 31772313]
40. Kwon OJ, Zhang L, Jia D, Zhou Z, Li Z, Haffner M et al. De novo induction of lineage plasticity from human prostate luminal epithelial cells by activated AKT1 and c-Myc. Oncogene 2020; 39: 7142–7151. [PubMed: 33009488]
41. Yoo YA, Vatapalli R, Lysy B, Mok H, Desouki MM, Abdulkadir SA. The Role of Castration-Resistant Bmi1+Sox2+ Cells in Driving Recurrence in Prostate Cancer. J Natl Cancer Inst 2019; 111: 311–321. [PubMed: 30312426]
42. Kar S, Sengupta D, Deb M, Pradhan N, Patra SK. SOX2 function and Hedgehog signaling pathway are co-conspirators in promoting androgen independent prostate cancer. Biochim Biophys Acta Mol Basis Dis 2017; 1863: 253–265. [PubMed: 27816521]
43. Zhang Z, Zhou C, Li X, Barnes SD, Deng S, Hoover E et al. Loss of CHD1 Promotes Heterogeneous Mechanisms of Resistance to AR-Targeted Therapy via Chromatin Dysregulation. Cancer Cell 2020; 37: 584–598 e511. [PubMed: 32220301]
44. Metz EP, Wuebben EL, Wilder PJ, Cox JL, Datta K, Coulter D et al. Tumor quiescence: elevating SOX2 in diverse tumor cell types downregulates a broad spectrum of the cell cycle machinery and inhibits tumor growth. BMC Cancer 2020; 20: 941. [PubMed: 32998722]
45. Hussenet T, Dali S, Exinger J, Monga B, Jost B, Dembelé D et al. SOX2 is an oncogene activated by recurrent 3q26. 3 amplifications in human lung squamous cell carcinomas. PloS one 2010; 5: e8960. [PubMed: 20126410]
46. Annovazzi L, Mellai M, Caldera V, Valente G, Schiffer D. SOX2 expression and amplification in gliomas and glioma cell lines. Cancer Genomics-Proteomics 2011; 8: 139–147. [PubMed: 21518820]
47. Bass AJ, Watanabe H, Mermel CH, Yu S, Perner S, Verhaak RG et al. SOX2 is an amplified lineage-survival oncogene in lung and esophageal squamous cell carcinomas. Nature genetics 2009; 41: 1238. [PubMed: 19801978]
48. Maier S, Wilbertz T, Braun M, Scheble V, Reischl M, Mikut R et al. SOX2 amplification is a common event in squamous cell carcinomas of different organ sites. Human pathology 2011; 42: 1078–1088. [PubMed: 21334718]
49. Wuebben EL, Rizzino A. The dark side of SOX2: cancer - a comprehensive overview. Oncotarget 2017; 8: 44917–44943. [PubMed: 28388544]
50. Cutruzzola F, Giardina G, Marani M, Macone A, Paiardini A, Rinaldo S et al. Glucose Metabolism in the Progression of Prostate Cancer. Front Physiol 2017; 8: 97. [PubMed: 28270771]
51. Varum S, Rodrigues AS, Moura MB, Momcilovic O, Easley Cat, Ramalho-Santos J et al. Energy metabolism in human pluripotent stem cells and their differentiated counterparts. PLoS One 2011; 6: e20914. [PubMed: 21698063]
52. Bergers G, Fendt SM. The metabolism of cancer cells during metastasis. Nat Rev Cancer 2021; 21: 162–180. [PubMed: 33462499]
53. Elia I, Doglioni G, Fendt SM. Metabolic Hallmarks of Metastasis Formation. Trends Cell Biol 2018; 28: 673–684. [PubMed: 29747903]
54. Whitburn J, Edwards CM. Metabolism in the Tumour-Bone Microenvironment. Current osteoporosis reports 2021; 19: 494–499. [PubMed: 34319488]
55. Zong WX, Rabinowitz JD, White E. Mitochondria and Cancer. Mol Cell 2016; 61: 667–676. [PubMed: 26942671]
56. Fraum TJ, Ludwig DR, Kim EH, Schroeder P, Hope TA, Ippolito JE. Prostate cancer PET tracers: essentials for the urologist. Can J Urol 2018; 25: 9371–9383. [PubMed: 30125515]
57. Jadvar H Is There Use for FDG-PET in Prostate Cancer? Semin Nucl Med 2016; 46: 502–506. [PubMed: 27825430]

58. Vander Griend DJ, Karthaus WL, Dalrymple S, Meeker A, DeMarzo AM, Isaacs JT. The role of CD133 in normal human prostate stem cells and malignant cancer-initiating cells. Cancer Res 2008; 68: 9703–9711. [PubMed: 19047148]

59. Wang MH, Shugart YY, Cole SR, Platz EA. A simulation study of control sampling methods for nested case-control studies of genetic and molecular biomarkers and prostate cancer progression. Cancer Epidemiol Biomarkers Prev 2009; 18: 706–711. [PubMed: 19258478]

60. Kregel S, Chen JL, Tom W, Krishnan V, Kach J, Brechka H et al. Acquired resistance to the second-generation androgen receptor antagonist enzalutamide in castration-resistant prostate cancer. Oncotarget 2016; 7: 26259–26274. [PubMed: 27036029]

61. Michiel Sedelaar JP, Dalrymple SS, Isaacs JT. Of mice and men--warning: intact versus castrated adult male mice as xenograft hosts are equivalent to hypogonadal versus abiraterone treated aging human males, respectively. Prostate 2013; 73: 1316–1325. [PubMed: 23775398]

62. Dracopoli NC. Current protocols in human genetics. Wiley: New York, NY, 1994, pp 2 volumes (loose-leaf).

63. Wang Q, Li W, Zhang Y, Yuan X, Xu K, Yu J et al. Androgen receptor regulates a distinct transcription program in androgen-independent prostate cancer. Cell 2009; 138: 245–256. [PubMed: 19632176]

64. Bolger AM, Lohse M, Usadel B. Trimmomatic: a flexible trimmer for Illumina sequence data. Bioinformatics 2014; 30: 2114–2120. [PubMed: 24695404]

65. Li H, Durbin R. Fast and accurate short read alignment with Burrows-Wheeler transform. Bioinformatics 2009; 25: 1754–1760. [PubMed: 19451168]

66. Zhang Y, Liu T, Meyer CA, Eeckhoute J, Johnson DS, Bernstein BE et al. Model-based analysis of ChIP-Seq (MACS). Genome Biol 2008; 9: R137. [PubMed: 18798982]

67. Bailey TL, Boden M, Buske FA, Frith M, Grant CE, Clementi L et al. MEME SUITE: tools for motif discovery and searching. Nucleic Acids Res 2009; 37: W202–208. [PubMed: 19458158]

68. Grant CE, Bailey TL, Noble WS. FIMO: scanning for occurrences of a given motif. Bioinformatics 2011; 27: 1017–1018. [PubMed: 21330290]

69. Mathelier A, Fornes O, Arenillas DJ, Chen CY, Denay G, Lee J et al. JASPAR 2016: a major expansion and update of the open-access database of transcription factor binding profiles. Nucleic Acids Res 2016; 44: D110–115. [PubMed: 26531826]

70. Wang L, Wang S, Li W. RSeQC: quality control of RNA-seq experiments. Bioinformatics 2012; 28: 2184–2185. [PubMed: 22743226]

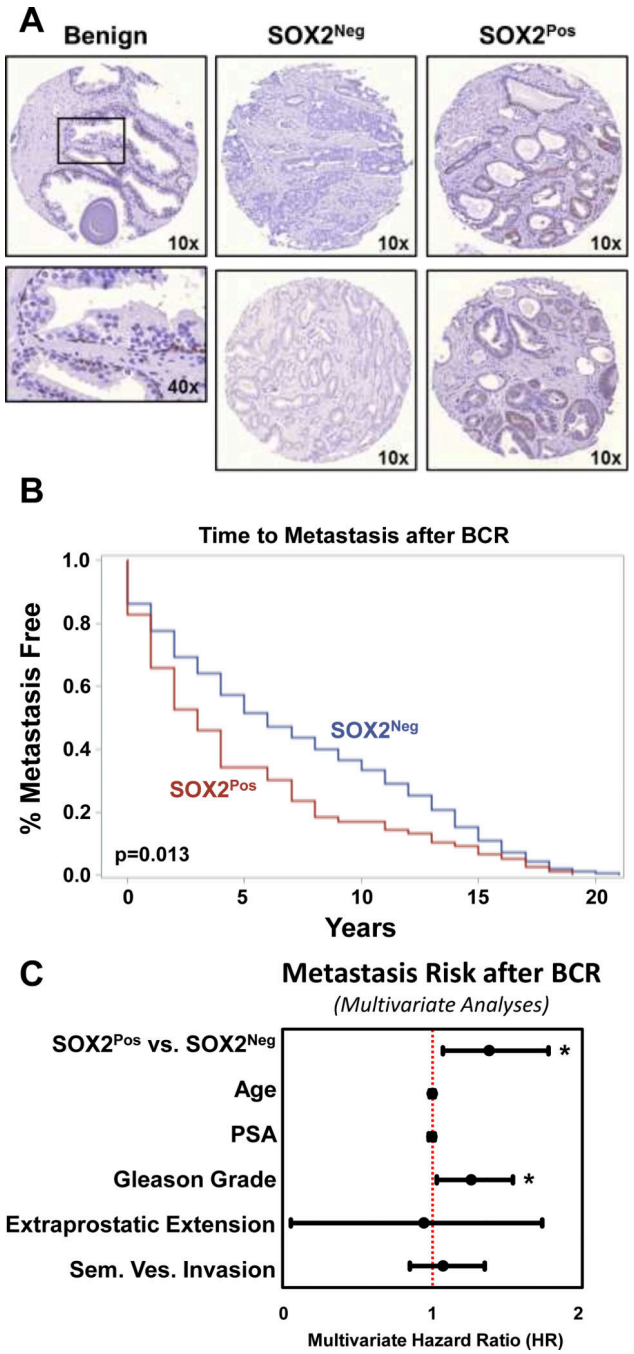

Figure 1: SOX2 Expression in Primary Prostate Tumors is Associated with Rapid Time to Metastasis and Prostate Cancer-Specific Mortality.

A) Representative images of SOX2 staining in prostate tissue. Benign glands (left panels) document basal epithelial staining (10x and 40x). SOX2-negative (middle panels) and SOX2-positive (right panels) tissues were scored and analyzed from a cohort of 726 annotated patient specimens (726-case PSA progression TMA). **B)** Kaplan-Meier curves of time to radiographic metastases after biochemical recurrence between SOX2-positive and SOX2-negative tumors after biochemical recurrence (BCR). **C)** Multivariate hazard ratios of metastasis risk between SOX2-positive and SOX2-negative tumors. Cox proportional-

hazards model combining age, PSA, Gleason grade, extraprostatic extension, and seminal vesicle invasion shows significant association with tumor SOX2 expression and metastasis risk in addition to the expected metastatic risk factors Gleason grade, extraprostatic extension, and seminal vesicle invasion. Bars represent 95% confidence intervals (*$p<0.05$).

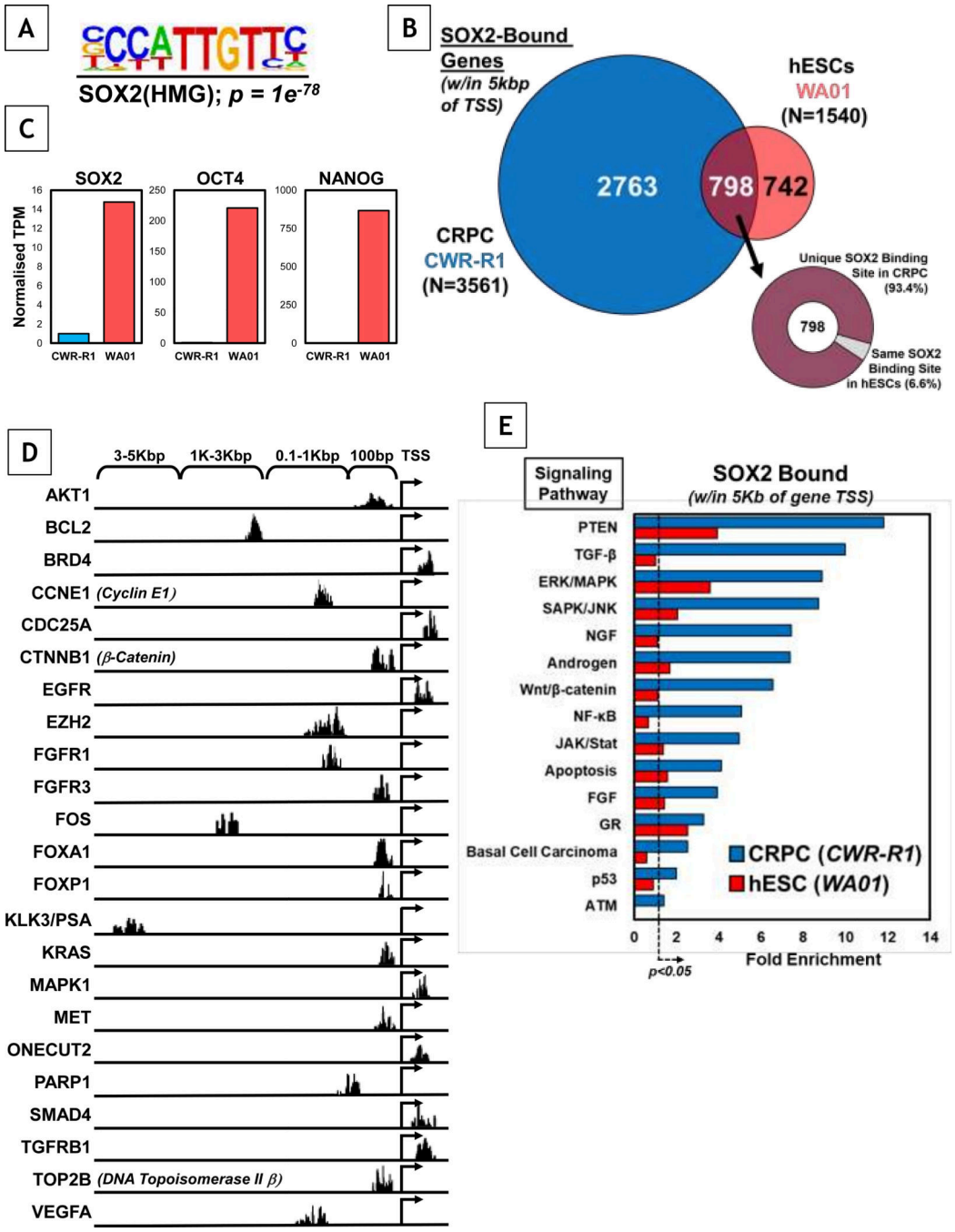

Figure 2: SOX2 ChIP-Seq in Castration-Resistant Prostate Cancer (CRPC) Cells Reveals Multiple Non-Stem Cell Gene Targets.

A) Motif analyses of SOX2 binding in CWR-R1 CRPC cells demonstrates canonical binding. **B)** Comparison of SOX2 binding sites between CWR-R1 CRPC cells and WA01 human embryonic stem cells (hESCs). Number represents binding within 5 kilobase pairs (5 kbp) of gene transcriptional start sites (TSS). Of the 798 overlapping SOX2 gene targets between CRPC cells and hESCs, 93.4% demonstrated unique SOX2 binding sites within the gene promoter (>10 bp apart), and only 6.6% had identical binding sites between cell types.

C) Comparison of mRNA expression of canonical stem cell transcription factors *SOX2*, *OCT4*, and *NANOG* in CWR-R1 CRPC cells and WA01 hESCs. Graphed as transcripts per million (TPM). Lack of detectable expression of *OCT4* and *NANOG* in CRPC cells suggests novel SOX2-binding partners in prostate cancer cells. **D)** Prostate cancer-specific SOX2 binding sites in CWR-R1 CRPC cells of genes of potential interest, many of which have documented roles in prostate cancer growth and progression. It should be noted that binding does not necessarily imply regulation. **E)** Pathway analyses comparing SOX2-bound genes in CWR-R1 CRPC cells and hESCs demonstrate potential differential cancer pathway regulation by SOX2 in prostate cancer cells.

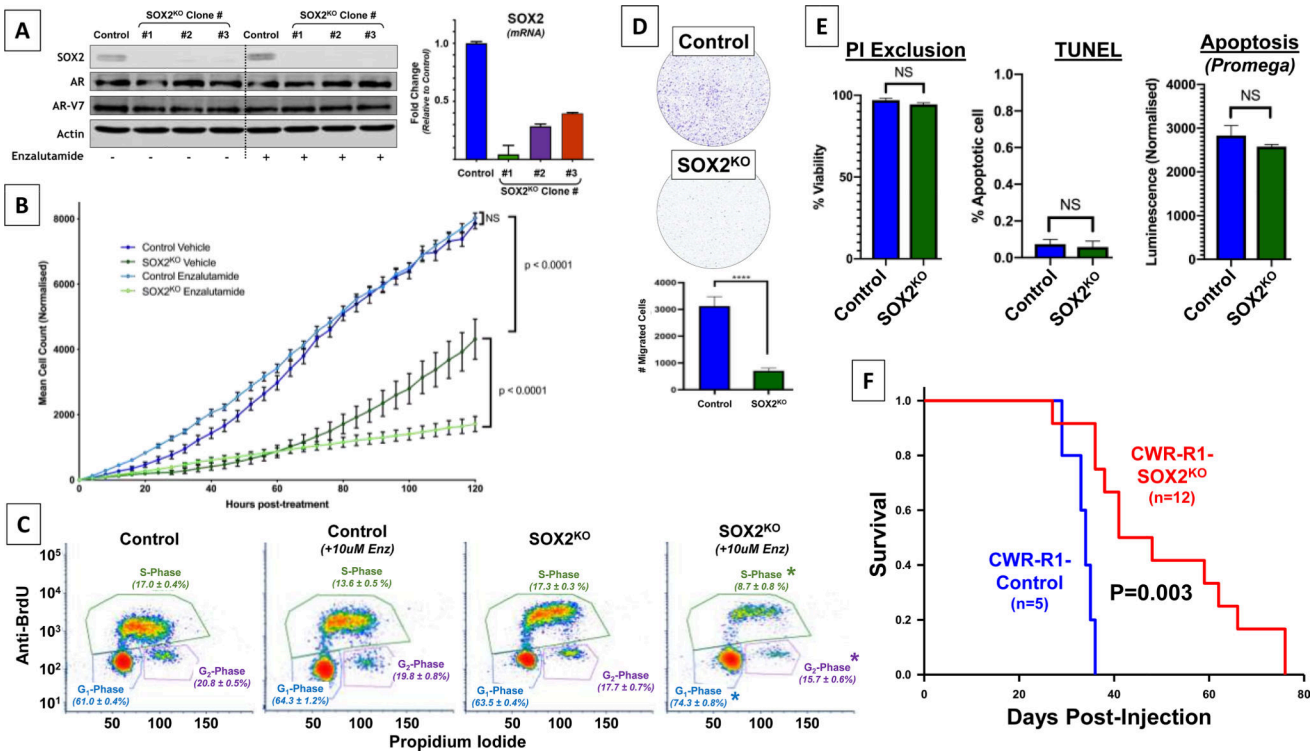

Figure 3: SOX2 Deletion in Castration-Resistant Prostate Cancer (CRPC) Cells Decreases Cell Growth and Invasion.

A) CRISPR-mediated deletion of SOX2 in CWR-R1 CRPC cells. Left panel: Western blot of three clonal lines of CWR-R1 CRPC cells with deleted SOX2 ($SOX2^{KO}$) in the absence and presence of the anti-androgen enzalutamide. Protein expression of androgen receptor (AR) and AR splice variant 7 (AR-V7) were unchanged. Actin was used as a loading control. Right panel: *SOX2* mRNA levels in the three clonal lines. Clone #1 was used for downstream analyses due to its very low *SOX2* mRNA expression and undetectable protein expression. **B)** Growth and sensitivity of $SOX2^{KO}$ cells. Growth curves of CWR-R1 CRPC cells (control) and CWR-R1-SOX^{KO} cells (SOX^{KO}) in the presence or absence of enzalutamide. **C)** Cell cycle distribution (BrdU incorporation vs. propidium iodide) of control and $SOX2^{KO}$ cells under normal growth conditions or upon treatment with enzalutamide (*$p<0.05$). **D)** Transwell migration of $SOX2^{KO}$ cells compared to control cells. Cells were plated in triplicate in transwell plates and were treated with aphidocolin to minimize effects of proliferation (*$p<0.05$). **E)** Comparison of cell viability or apoptosis of control vs. $SOX2^{KO}$ CWR-R1 CRPC cells in propidium iodide (PI) exclusion, TUNEL, and apoptosis assays (NS=not significant). **F)** Kaplan-Meier curves of survival of hormonally-intact male nude mice with xenografts of CWR-R1-control or $SOX2^{KO}$ cells.

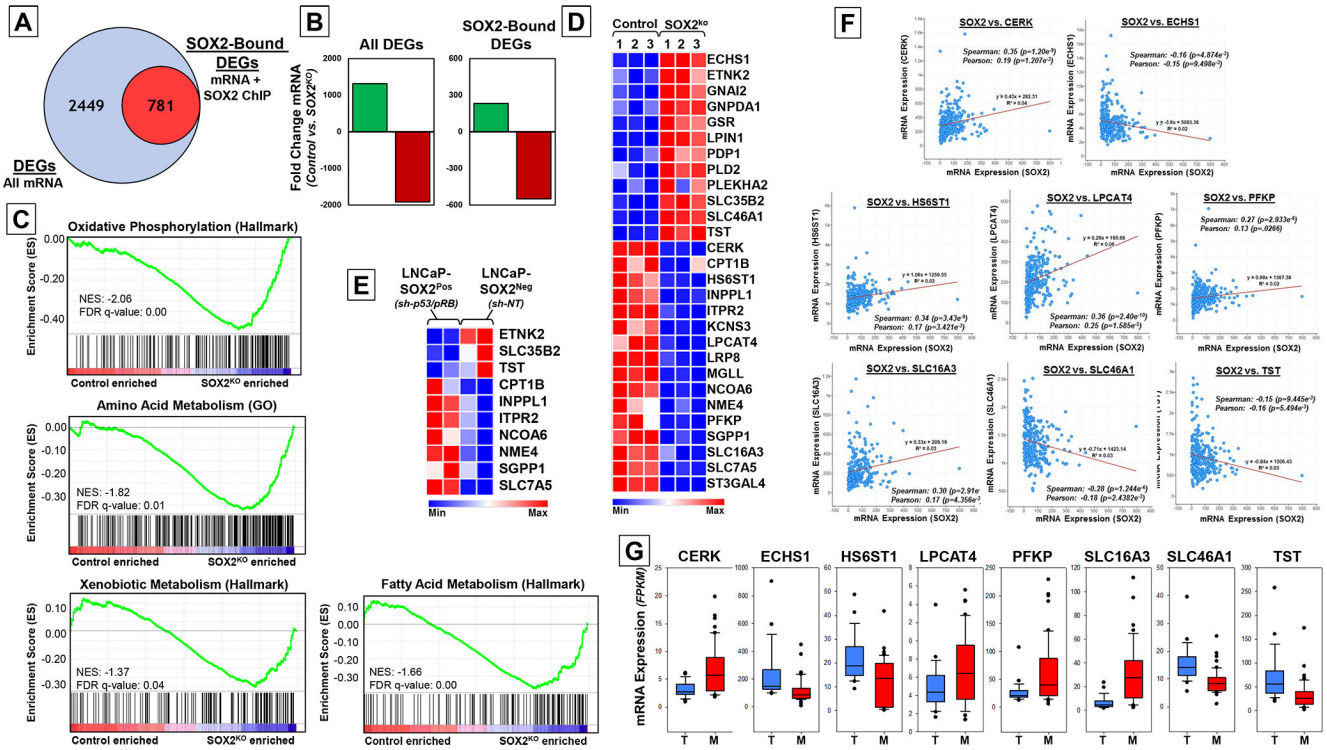

Figure 4: SOX2 is Associated with Changes in Cellular Metabolism in Prostate Cancer Cells, Tumors, and Metastases.

A) Comparative RNA-Seq analyses of CWR-R1-Control vs. SOX2^{KO} cells. Differentially expressed genes (DEGs) between control and SOX2^{KO} cells document 2,449 total genes differentially expressed by >1.5-fold. Additional analyses of SOX2 ChIP-Seq data demonstrate a cohort of 781 genes that were SOX2-bound (ChIP-Seq) and differentially expressed when SOX2 was deleted (RNA-Seq). **B)** Directional analyses of DEGs, including SOX2-bound DEGs, upon SOX2 deletion. **C)** Gene Set Enrichment Analysis (GSEA) of RNA-Seq datasets prioritizes multiple pathways associated with cellular metabolism. **D)** Heatmap of SOX2-bound genes prioritized using GSEA Leading Edge analyses. Data represent TPM values of RNA-Seq triplicates. **E)** Comparative analyses of SOX2-positive vs. SOX2-negative LNCaP cells with reduced RB and p53 expression also document changes in metabolic-associated SOX2-bound genes. **F)** Clinical correlation of SOX2-bound DEGs involved in metabolism using publicly available TCGA data. Data demonstrate significant and directional correlation between *SOX2* mRNA expression and prioritized metabolic SOX2-target genes. **G)** Analyses of mRNA expression of metabolic SOX2-target genes between prostate tumors and metastases. Values represent mean fragments per kilobase of transcript per million mapped reads (FPKM) expression from RNA-Seq data from tumors (n=25) and metastases (N=53).

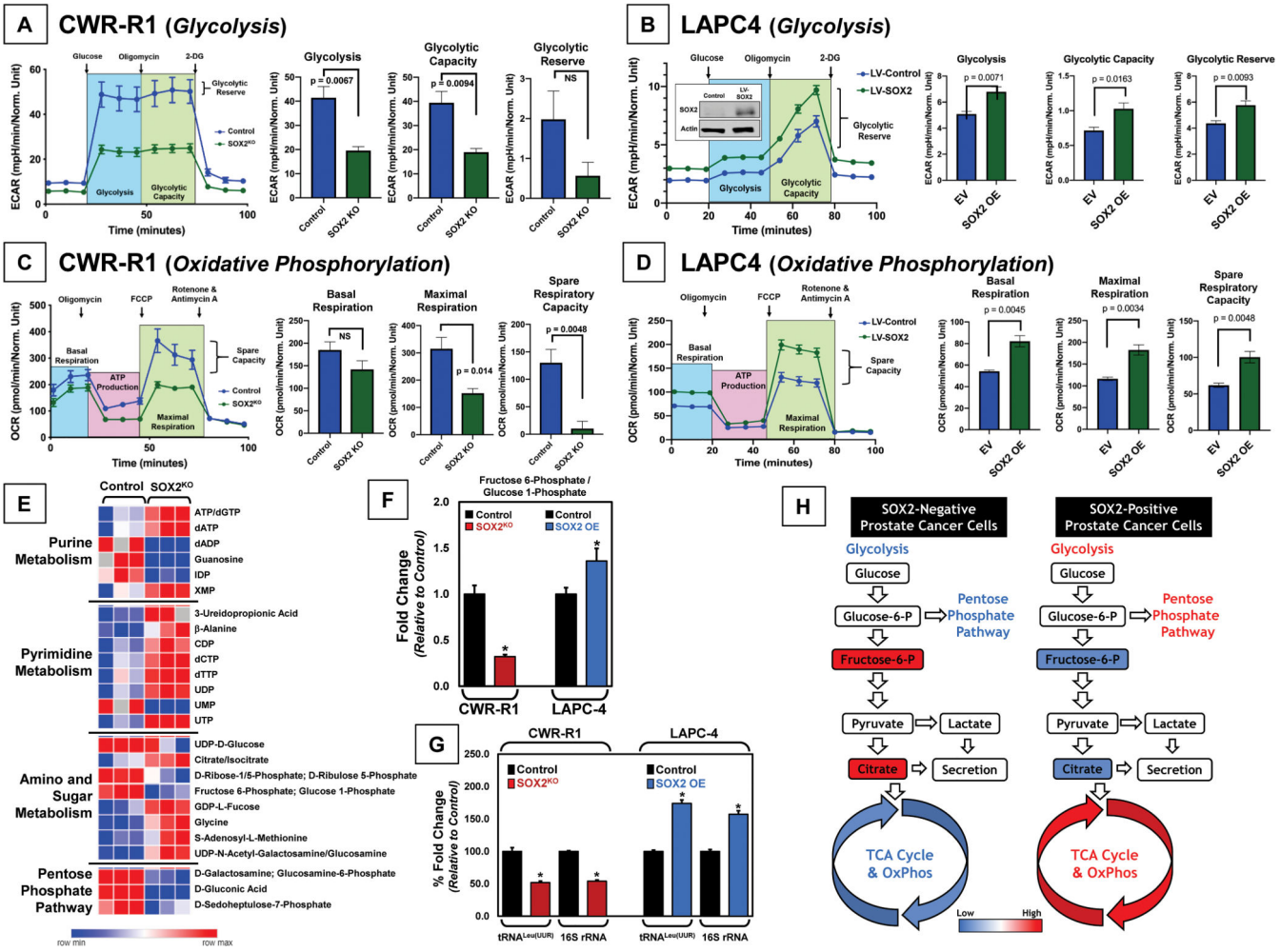

Figure 5: SOX2 Expression Promotes Increased Glycolysis, Oxidative Phosphorylation, and Mitochondrial Quantity.

A) Seahorse Glycolysis Stress Test comparing CWR-R1-Control vs. SOX2^{KO} cells. Extracellular acidification rate (ECAR) was measured as glucose, oligomycin, and 2-DG were added sequentially. Data and p-values represent triplicate experiments. **B)** Seahorse Glycolysis Stress Test comparing LAPC4-Control vs. LAPC4-LV-SOX2 (lentiviral SOX2 over-expressing cells, or SOX2-OE). Data and p-values represent triplicate experiments. **C)** Seahorse Mito Stress Test comparing CWR-R1-Control vs. SOX2^{KO} cells. Oxygen consumption rate (OCR) was measured as oligomycin, FCCP, and rotenone/antimycin A were added sequentially. Data and p-values represent triplicate experiments. **D)** Seahorse Mito Stress Test comparing LAPC4-Control vs. LAPC4-LV-SOX2 (SOX2-OE). Data and p-values represent triplicate experiments. **E)** Metabolomic analyses of control and SOX2^{KO} CWR-R1 cells for changes in purine, pyrimidine, amino acid, and sugar metabolism, as well as changes in the pentose-phosphate pathway. Data represent normalized fold-change to control values of triplicate analyses. **F)** SOX2-associated changes in fructose-6-phosphate/glucose-1-phosphate in control and SOX2^{KO} CWR-R1 cells as well as control and SOX2-OE LAPC4 cells (*p<0.05). **G)** Quantitative PCR of SOX2-associated changes in mitochondria quantity measured as mitochondrial-specific tRNA$^{Leu(UUR)}$ and 16S rRNA

between control and SOX2^{KO} CWR-R1 cells as well as control and SOX-OE LAPC4 cells. **H)** Schematic of SOX2-regulated changes in prostate cancer cell metabolism. SOX2-negative cells have decreased glycolysis, decreased pentose phosphate pathway activity, decreased fructose-6-phosphate, increased citrate, and decreased TCA cycle and oxidative phosphorylation. SOX2 expression leads to increased glycolysis, increased pentose phosphate pathway activity, increased fructose-6-phosphate, decreased citrate, and increased TCA cycle and oxidative phosphorylation.

Table 1:

Post-Operative Outcomes Between $SOX2^{Pos}$ and $SOX2^{Neg}$ Tumors

	$SOX2^{Pos}$ ***(N=123)***	**$SOX2^{Neg}$** ***(N=602)***	**P-value**
BCR (%)	71.5%	70.4%	0.6708
Years to BCR (Mean ± SD)	2.39 ± 1.90	2.64 ± 1.94	0.104
PSA at Surgery (Mean ± SD)	10.97 ± 9.71	11.67 ± 9.31	0.085
Gleason Grade Post-RP (%)			0.0870
GG6	13.8%	15.9%	
GG3+4	44.7%	39.4%	
GG4+3	20.3%	16.9%	
GG8	13.0%	13.3%	
GG9–10	8.1%	11.8%	
Surgical Margin (%)			0.9373
Negative	68.3%	68.3%	
Positive	31.7%	31.7%	
Pathological Extension (%)			
Organ Confined	17.1%	16.4%	0.1060
Extraprostatic	81.3%	79.2%	0.4802
Lymph Node Positive	19.5%	15.4%	0.293
Local Recurrence (%)	15.4%	14.0%	0.408
Salvage Treatment (%)[a]	57.7%	64.6%	0.1486
Years to Salvage Treatment (Mean ± SD)	5.06 ± 5.69	6.01 ± 6.87	0.608
Metastases After BCR (%)	51.3%	43.0%	0.127
Time to Metastases after BCR (Mean ± SD)	7.59 ± 5.39	9.85 ± 6.58	**<0.001**
Cancer Specific Survival (%)			**0.0138**
Alive	72.4%	80.9%	
Dead from PCa	27.6%	19.1%	
Overall Death (%)	45.5%	34.1%	**0.018**

a: Includes salvage ADT, radiation, or both.